Results in Physics 8 (2018) 502–512

Contents lists available at ScienceDirect

Results in Physics

journal homepage: www.journals.elsevier.com/results-in-physics

Analysis of activation energy in Couette-Poiseuille flow of nanofluid in the presence of chemical reaction and convective boundary conditions

A. Zeeshan, N. Shehzad *, R. Ellahi

Department of Mathematics and Statistics, FBAS, International Islamic University, Islamabad 44000, Pakistan

ARTICLE INFO

Article history:
Received 2 November 2017
Received in revised form 6 December 2017
Accepted 10 December 2017
Available online 28 December 2017

Keywords:
Convective boundary conditions
Activation energy
Chemical reaction
Couette-Poiseuille flow
Thermal radiation
Nanofluid

ABSTRACT

The motivation of the current article is to explore the energy activation in MHD radiative Couette-Poiseuille flow nanofluid in horizontal channel with convective boundary conditions. The mathematical model of Buongiorno [1] effectively describes the current flow analysis. Additionally, the impact of chemical reaction is also taken in account. The governing flow equations are simplified with the help of boundary layer approximations. Non-linear coupled equations for momentum, energy and mass transfer are tackled with analytical (HAM) technique. The influence of dimensionless convergence parameter like Brownian motion parameter, radiation parameter, buoyancy ratio parameter, dimensionless activation energy, thermophoresis parameter, temperature difference parameter, dimensionless reaction rate, Schmidt number, Brinkman number, Biot number and convection diffusion parameter on velocity, temperature and concentration profiles are discussed graphically and in tabular form. From the results, it is elaborate that the nanoparticle concentration is directly proportional to the chemical reaction with activation energy and the performance of Brownian motion on nanoparticle concentration gives reverse pattern to that of thermophoresis parameter.

Introduction

Nanofluids are the colloidal suspensions of nanomaterials which are prepared by inclusion of nanometer-sized materials, (i.e., nanoparticles, nanowires, nanotubes, nanorods and nanofibers) along with the base fluids. Water, oil and ethylene glycol are commonly used base fluids. Choi et al. [2] introduced the concept of nanofluids in order to generate fluids with heat transfer rate and higher thermal conductivity. Nanofluids have extraordinary characteristics that make them potentially useful. Due to the wide range of applications they after received significant attention. Nanofluids are used as cooling agent in electronic equipment, vehicles, heavy-duty engine and in industries to enhance the efficiency, save energy and reduce emissions. Nanofluids have also some biomedical applications, like in antibacterial and drug delivery. Consequently, nanofluids represent an area of interest for many scientists and researchers due to numerous applications. Some of the recent explorations may include study by Sheikholeslami and Ganji [3] who investigated numerically the flow of nanofluid containing copper nanoparticles in the presence of uniform magnetic field effect. Rashidi et al. [4] found an analytic and numerical solution of viscous water based nanofluid with second order slip condition using fourth order RK method together with shooting iteration method. He noticed that when turbulent effects are absent, the thermophoresis and Brownian diffusion are the most important factors for determination of the characteristics of nanofluids. He then established the conservation equations contained with these two effects. Also based on these two dominant factors, Shehzad et al. [5] introduced Buongiorno's [1] model for heat and mass transport in a channel flow for nanofluid using Homotopy analysis method. Xu et al. [6] used Buongiorno mathematical model in vertical channel to discuss the analysis of mixed convection flow of a nanofluid. Authors investigated that the characteristic of heat transfer can be improved if the suitable nanofluid used. Some recent contributions are made by a number of researchers [7–13] over diverse geometries.

The study of magnetic field effects has important applications in physics, chemistry and engineering. Industrial equipment, such as magnetohydrodynamic (MHD) generators, pumps, bearings and boundary layer control are affected by the interaction between the electrically conducting fluid and a magnetic field. The work of many investigators has been studied in relation to these applications. One of the basic and important problems in this area is the hydromagnetic behavior of boundary layers along fixed or moving surfaces in the presence of a transverse magnetic field. The impact

* Corresponding author.
E-mail address: nasir.isbrwp@gmail.com (N. Shehzad).

https://doi.org/10.1016/j.rinp.2017.12.024
2211-3797/© 2017 The Authors. Published by Elsevier B.V.

Nomenclature

$\boldsymbol{V}$	Dimensional nanofluid velocity [$m\,s^{-1}$]
$\boldsymbol{T}$	Dimensional nanofluid temperature [K]
$\boldsymbol{C}$	Dimensional nanoparticle concentration [K]
$\bar{u}, \bar{v}$	Dimensional components of velocity along $\bar{x}$ and $\bar{y}$ [$m\,s^{-1}$]
$\bar{p}$	Dimensional pressure [$N\,m^{-2}$]
$\boldsymbol{B}$	Magnetic field strength
u, v	Dimensionless components of velocity along x and y
$2a$	Width of channel [m]
k	Thermal conductivity [$W\,m^{-1}\,K^{-1}$]
D_T	Thermophoretic diffusion coefficient [$m^2\,s^{-1}$]
D_B	Brownian diffusion coefficient [$m^2\,s^{-1}$]
K_r^2	Reaction rate
B_0	Uniform transverse magnetic field [T]
h_f	Heat transfer coefficient
n	Temperature scale
k^*	Mean absorption coefficient
P	Constant pressure gradient
Ra	Rayleigh number for the porous medium
M	Magnetic field parameter
Rd	Radiation parameter
N_b	Brownian motion parameter
N_r	Buoyancy ratio
Re	Reynolds number
Br	Brinkman number
C_p	Heat capacity [$J\,kg^{-1}K^{-1}$]
C_f	Skin friction coefficient

Greek symbols

μ	Dynamic Viscosity [$Ns\,m^{-2}$]
$(\rho C_p)_f$	Heat capacity of the base fluid [$J\,K^{-1}m^{-3}$]
ε	Momentum accommodation coefficient
α	Thermal diffusivity $\frac{k}{(\rho C)_f}$ [$m^2\,s^{-1}$]
β	Volumetric volume expansion coefficient [K^{-1}]
$(\rho C_p)_s$	Effective heat capacity of the nanoparticle material [$J\,K^{-1}m^{-3}$]
τ	Parameter defined by $\frac{(\rho C_p)_s}{(\rho C_p)_f}$

Subscripts

f	Base fluid
T_1	Lower wall temperature [K]
T_2	Upper wall temperature [K]
$\boldsymbol{g}$	Gravitational acceleration [$m\,s^{-2}$]
T^*	Mean temperature of T_1 and T_2
C_1	Lower wall concentration [K]
C_2	Upper wall concentration [K]
C^*	Mean concentration of C_1 andC_2
$\boldsymbol{J}$	Joule current [$C\,m^{-3}$]
Φ	Viscous dissipation
q_r	Radiative heat flux
E_a	Activation energy
κ	Boltzmann constant
n_1	Fitted rate constant
h_s	Mass transfer coefficient
m	Concentration scale
p	Dimensionless pressure
Pr	Prandtl number
E_c	Eckert number
N_t	Thermophoresis parameter
S_c	Schmidt number
Bi	Biot number
Nj	Convection diffusion parameter
Λ	Reaction rate
E	Activation energy,
Sh	Sherwood number
Nu	Nusselt number
ν	Kinematic viscosity [$m^2\,s^{-1}$]
θ	Dimensionless temperature
ϕ	Nanoparticle concentration
σ^*	Stefan Boltzman constant
σ	Electrical conductivity [Sm^{-1}]
ρ	Density [$kg\,m^{-3}$]
δ	Temperature difference parameter
s	Nanoparticle material

of MHD nanofluid forced convection in a lid driven porous cavity is discussed by Sheikholeslami [14]. The author gives the Outputs indicate that selecting Platelet shaped nanoparticles results the highest heat transfer rate. Nusselt number augments with rise of Darcy and Reynolds number while it decreases with augment of Lorentz forces. Bhatti et al. [15] investigated the entropy generation with combined effects of thermal radiation and chemical reaction on MHD boundary layer over a moving surface. MHD mixed convective heat transfer for an incompressible, laminar, and electrically conducting viscoelastic fluid flow past a permeable wedge with thermal radiation is analytically and numerically discussed by Rashidi et al. [16]. In another study Rashidi et al. [17] discussed the entropy generation analysis of flow and heat transfer in an incompressible nanofluid flowing over a rotating porous disk in the presence of an MHD effect for three different types of nanoparticles: Cu, CuO and Al2O3. The authors obtained the fundamental objective of the second law thermodynamics analysis that the minimization of entropy in the swirling disk flow regime, when the magnetic interaction parameter, suction parameter and nanoparticle volume fraction decreased. The impact of shape factor on nanofluid forced convection in a porous semi-annulus is studied in presence of uniform MHD by Sheikholeslami and Bhatti [10]. It is observed that platelet shape has greatest heat transfer rate. Moreover, due to the augmentation of nanofluid volume fraction, Reynolds and Darcy number, Nusselt number increases whereas it reduces due to the increment in Lorentz forces. Convective limit condition is for the most part used to characterize a straight convective energy transport condition for at least one logarithmic elements in energy. Energy exchange investigation with convective limit conditions is evoked in procedures, for example, energy vitality stockpiling, gas turbines, atomic plants, and so on. Ramesh and Gireesha [18] built up a model for the impact of energy source/sink on Maxwell nanofluids on extending surface under the nearness of convective limit conditions. The impacts of energy source/ingestion on stagnation point stream of nanofluid on the surface affected by convective limit conditions was contemplated by Alsaedi et al. [19]. Zeeshan et al. [20] designates the effects of thermal radiation and viscous dissipation parameter for multiphase magnetic fluid over a stretching surface. The result illustrated that the temperature is increasing for PST and PHF with the increase of thermal radiation but viscous dissipation parameter gives the opposite trend on temperature profile for both cases. Hamad et al. [21]

discussed the joined impacts of heat and mass exchange on a penetrable level surface with the existence of MHD with convective surface conditions. The entropy analysis for nanofluid flow through vertical channel having MHD and nonlinear radiation behavior with convective surface conditions is discussed by Lopez et al. [22].

The process of mass transfer analysis with Arrhenius activation energy and chemical reaction has been given a lot of attention due to its various applications in chemical engineering, cooling of nuclear reacting, geothermal reservoirs, and recovery of thermal oil. Generally, the relations of chemical reaction with mass transfer are very difficult, and it can be scrutinized in the utilization of reactant species and production at several rates within the mass transfer of nanofluid. Bestman [23] was the first to consider the mutual performance of the chemical reaction with Arrhenius activation energy for convective mass transfer in a vertical pipe immersed with porous media. He used perturbation method to obtain analytical solution. Maleque [24] studied free convection MHD flow and heat with mass transfer over a porous vertical plate with binary chemical reaction and Arrhenius activation energy with heat generation \ absorption and viscous dissipation. Mustafa et al. [25] discussed the chemical reaction and activation energy with buoyancy effects on magneto-nanofluid passed through a vertical surface. Researchers agreed to make decision that the concentration of nanoparticle with chemical reaction and activation energy is proportional to each other and the effects of thermophoresis parameter on nanoparticle concentration is opposite to that of Brownian motion. The effects of MHD flow in convergent and divergent channels are investigated by Mohyud-Din et al. [26]. Authors concluded that the concentration profile gives the decreasing effect with the increase of Reynolds number in divergent channel while it increase in convergent channel with the increase of Reynolds number. Mousavi et al. [27] explored the viscous flow as well as heat transfer using two-equation energy model inside a channel fixed in porous media. The unsteady flow with heat and mass transfer past a stretching sheet with chemical reaction with Arrhenius activation energy in a rotating fluid was scrutinized by Awad et al. [28]. Recently, Shafique et al. [29] studied the steady flow of a non-Newtonian Maxwell fluid past an elastic surface in a rotating frame in the presence of binary chemical reaction along with the activation energy.

In the review of literature survey it examined that there is no such investigation has been reported in a Couette–Poiseuille nanofluid flow through two parallel straight walls with convective boundary heat and mass conditions. The purpose of current study is to scrutinize the mutual influence of chemical reaction with activation energy and manufacturing extrusion thermal system in the presence of radiation effects. For this problem we apply similarity transformations on the partial, differential equations. The governing systems of highly nonlinear coupled ordinary, differential equations are tackled analytically with the advantages of homotopy analysis method (HAM) [30–32]. The solutions obtained by HAM has the following advantages. (i) HAM does not require any small/large parameters in the problem. (ii) It gives us a way to verify the convergence of the developed series solutions. (iii) It is useful in providing flexibility in the developing equation of linear functions of solutions. On the other hand it may take unnecessary long computational time and some time for complex problems solution could not achieved desired convergences as computers may not have sufficient internal memory. The following sections consist of problem formulation, solution procedure, convergence analysis, results and discussion, conclusion and references. Also the fallouts of velocity, temperature together with skin friction and Nusselt number are briefly nattered for the concerned parameters.

Problem formulation

Here consider an unsteady fully developed laminar flow of incompressible nanofluid passing through a horizontal channel. The geometry of the channel consist two parallel infinite walls as shown in Fig. 1. The upper wall is supposed to move with a constant velocity U^*, whereas the lower wall is stationary.

We consider the Couette-Poiseuille flow with constant pressure gradient. In the geometry of the problem, the middle of the channel is taken at origin with position of walls at $\bar{y} = -a$ and $\bar{y} = a$, respectively. Concerned problem is consider in Cartesian coordinate system, such that $\bar{x}$-axis is taken along the channel wall, while $\bar{y}$-axis is perpendicular to the channel and parallel to the gravitational acceleration vector $\boldsymbol{g}$ but with the opposite direction. Convective boundary conditions are subject to lower and upper wall of the channel. Fluid is taken electrically conducted with non-uniform magnetic field $\boldsymbol{B}$ in the $\bar{y}$-direction (see Fig. 1). Hall current and electric field are considered to be negligible for small Reynolds number. The physical properties of nanofluid in this problem are supposed constant.

Under the above considerations, the conservations equations for mass (continuity), momentum (velocity), thermal (energy) and concentration (nanoparticles) can be defined as follows (see Mustafa et al. [33] for details):

$$\nabla.\boldsymbol{V} = 0, \tag{1}$$

$$\rho_f(\boldsymbol{V}.\nabla)\boldsymbol{V} = -\nabla\bar{p} + \mu\nabla^2\boldsymbol{V} + [\boldsymbol{C}\rho_s + \rho_f(1-\boldsymbol{C})(1-\beta(\boldsymbol{T}-T^*))]\boldsymbol{g} + \boldsymbol{J}\times\boldsymbol{B}, \tag{2}$$

$$(\rho C_p)_f(\boldsymbol{V}.\nabla)\boldsymbol{T} = k\nabla^2\boldsymbol{T} + (\rho C_p)_s\left[\left(\frac{D_T}{T^*}\right)\nabla\boldsymbol{T}.\nabla\boldsymbol{T} + D_B\nabla\boldsymbol{C}.\nabla\boldsymbol{T}\right] + \Phi - \nabla.q_r + \frac{1}{\sigma}\boldsymbol{J}\boldsymbol{J}, \tag{3}$$

$$\rho_s(\boldsymbol{V}.\nabla)\boldsymbol{C} = -\nabla.\mathbf{j}_s - \rho_s K_r^2\left(\frac{\boldsymbol{T}}{T^*}\right)^{n_1}(\boldsymbol{C}-C^*)\exp\left(\frac{-E_a}{\kappa\boldsymbol{T}}\right). \tag{4}$$

Here $\mathbf{j}_s = -\rho_s\{D_B\nabla\boldsymbol{C} + (D_T/T^*)\nabla\boldsymbol{T}\}$ is the nanoparticles mass flux defined by Revnic et al. [34], magnetic field strength is $\boldsymbol{B} = [0, B_0, 0]$, $\boldsymbol{J} = \sigma(\boldsymbol{V}\times\boldsymbol{B})$ is the current density in which σ electrical conductivity of nanofluid, $\boldsymbol{g} = (0, g, 0)$ is the gravitational acceleration. The term $K_r^2(\boldsymbol{T}/T^*)^{n_1}\exp(-E_a/\kappa\boldsymbol{T})$ in Eq. (4) describes the chemical reaction with activation energy usually called modified Arrhenius function [35]. $\kappa = 8.61\times10^{-5}$ eV/K is the Boltzmann constant, n_1 is the fitted rate constant generally lies between $-1 < n_1 < 1$. Here employing the Buongiorno [1] nanofluid model and then introducing the Oberbeck–Boussinesq approximation with the boundary layer approximation on it as done by Kuznetsov and Nield [36]. Hence the above said fields Eqs. (1) to (4) can be described in components form:

$$\frac{\partial\bar{u}}{\partial\bar{x}} + \frac{\partial\bar{v}}{\partial\bar{y}} = 0, \tag{5}$$

$$\frac{\partial\bar{p}}{\partial\bar{x}} = \mu\frac{\partial^2\bar{u}}{\partial\bar{y}^2} - \sigma B_0^2\bar{u} + [(1-C^*)\rho_f\beta(\boldsymbol{T}-T^*) + (\rho_s-\rho_f)(\boldsymbol{C}-C^*)]g, \tag{6}$$

$$\bar{u}\frac{\partial\boldsymbol{T}}{\partial\bar{x}} = \alpha\left(\frac{\partial^2\boldsymbol{T}}{\partial\bar{y}^2}\right) + \tau\left[\frac{D_T}{T^*}\left(\frac{\partial\boldsymbol{T}}{\partial\bar{y}}\right)^2 + D_B\frac{\partial\boldsymbol{C}}{\partial\bar{y}}\frac{\partial\boldsymbol{T}}{\partial\bar{y}}\right] + \frac{\mu}{(\rho C_p)_f}\left(\frac{\partial\bar{u}}{\partial\bar{y}}\right)^2 + \frac{\sigma B_0^2}{(\rho C_p)_f}\bar{u}^2 - \frac{1}{(\rho C_p)_f}\frac{\partial q_r}{\partial\bar{y}}, \tag{7}$$

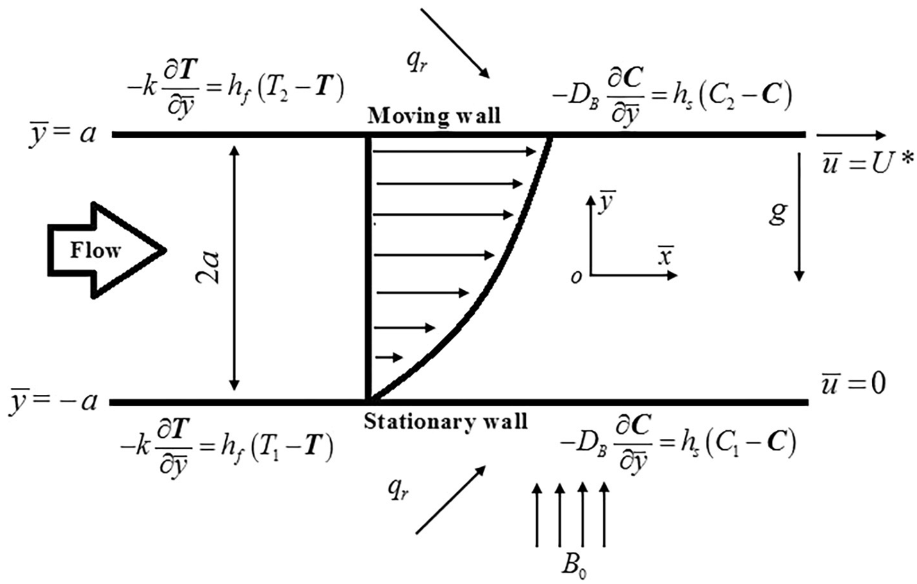

Fig. 1. A physical sketch of flow problem.

$$-D_B \frac{\partial^2 \boldsymbol{C}}{\partial \bar{y}^2} = \left(\frac{D_T}{T^*}\right) \frac{\partial^2 \boldsymbol{T}}{\partial \bar{y}^2} - K_r^2 \left(\frac{\boldsymbol{T}}{T^*}\right)^{n_1} (\boldsymbol{C} - C^*) \exp\left(\frac{-E_a}{\kappa \boldsymbol{T}}\right). \tag{8}$$

The appropriate Couette-Poiseuille and convective boundary conditions are:

$$\begin{aligned} &\bar{u} = U^*,\ \bar{v} = 0,\ -k\frac{\partial \boldsymbol{T}}{\partial \bar{y}} = h_f(T_2 - \boldsymbol{T}),\ -D_B\frac{\partial \boldsymbol{C}}{\partial \bar{y}} = h_s(C_2 - \boldsymbol{C}) \quad \text{at } \bar{y} = a \\ &\bar{u} = 0,\ \bar{v} = 0,\ -k\frac{\partial \boldsymbol{T}}{\partial \bar{y}} = h_f(T_1 - \boldsymbol{T}),\ -D_B\frac{\partial \boldsymbol{C}}{\partial \bar{y}} = h_s(C_1 - \boldsymbol{C}) \quad \text{at } \bar{y} = -a \end{aligned} \tag{9}$$

Now Eqs (5) to (8) and boundary conditions (9) can be converted into a dimensionless form with the help of following dimensionless variables:

$$\begin{aligned} &x = \frac{\bar{x}}{a},\quad u = \frac{\bar{u}}{U_m},\quad \theta = \frac{\boldsymbol{T} - T*}{T_1 - T*},\quad n = \frac{T_2 - T*}{T_1 - T^*},\quad p = \frac{a^2 \bar{p}}{\mu U_m}, \\ &y = \frac{\bar{y}}{a},\quad v = \frac{\bar{v}}{U_m},\quad \phi = \frac{\boldsymbol{C} - C^*}{C_1 - C^*},\quad m = \frac{C_2 - C^*}{C_1 - C^*},\quad U = \frac{U^*}{U_m}. \end{aligned} \tag{10}$$

As flow direction is along x-axis, therefor the velocity component along y-axis is zero i.e. $v = 0$. The continuity equation remain $\frac{\partial u}{\partial x} = 0$, which implies $u = u(y)$ and from momentum equation $\frac{\partial p}{\partial y} = 0$, which shows $p = p(x)$, also consider $\frac{\partial p}{\partial x} = P$ (constant). Fluid flow is due to the constant pressure gradient. Here it is supposed that the maximum velocity $\left(U_m = -\frac{a^2}{2\mu}\frac{\partial p}{\partial x}\right)$ occurred between two walls. n, m are the temperature and concentration scale respectively and both are taken to zero in this case. The radiative heat flux q_r is described by Rosseland approximation [37], i.e.

$$q_r = -\frac{4\sigma^*}{3k^*} \frac{\partial \boldsymbol{T}^4}{\partial \bar{y}}. \tag{11}$$

In this phenomena it considered that the difference of temperature with in the flow is very small, so that $\boldsymbol{T}^4$ expressed the linear function of simple temperature. Expended $\boldsymbol{T}^4$ by Taylor series about Mean value temperature T^* as below:

$$\boldsymbol{T}^4 = T^{*4} + 4T^{*3}(\boldsymbol{T} - T^*) + 6T^{*2}(\boldsymbol{T} - T^*)^2 + \cdots \tag{12}$$

Eq. (12) becomes after neglecting $(\boldsymbol{T} - T^*)^2$ and higher-order terms:

$$\boldsymbol{T}^4 \cong 4T^{*3}\boldsymbol{T} - 3T^{*4} \tag{13}$$

Thus, Eq. (11) becomes after substituting Eq. (13), we have:

$$q_r = -\frac{16T^{*3}\sigma^*}{3k^*} \frac{\partial \boldsymbol{T}}{\partial \bar{y}} \tag{14}$$

By using Eq. (10), the non-dimensional form of Eqs. (5) to (8) can be stated:

$$\frac{\partial^2 u}{\partial y^2} - M^2 u + \frac{Ra}{\mathrm{Re}\,\mathrm{Pr}}(\theta - Nr\phi) - P = 0, \tag{15}$$

$$(1 + Rd)\frac{\partial^2 \theta}{\partial y^2} + Nb\frac{\partial \theta}{\partial y}\frac{\partial \phi}{\partial y} + Nt\left(\frac{\partial \theta}{\partial y}\right)^2 + Br\left(\frac{\partial u}{\partial y}\right)^2 + M^2 Bru^2 - \gamma u = 0, \tag{16}$$

$$\frac{\partial^2 \phi}{\partial y^2} + \frac{Nt}{Nb}\left(\frac{\partial^2 \theta}{\partial y^2}\right) - S_c\,\mathrm{Re}\Lambda(1 + \delta\theta)^{n_1} \exp\left(-\frac{E}{(1 + \delta\theta)}\right) = 0. \tag{17}$$

The corresponding dimensionless boundary conditions:

$$\begin{aligned} &u = U,\quad v = 0,\quad \theta'(y) = -Bi(n - \theta(y)), \\ &\phi'(y) = -Nj(m - \phi(y)) \quad \text{at } y = 1 \end{aligned} \tag{18}$$

$$\begin{aligned} &u = 0,\quad v = 0,\quad \theta'(y) = -Bi(1 - \theta(y)), \\ &\phi'(y) = -Nj(1 - \phi(y)) \quad \text{at } y = -1, \end{aligned} \tag{19}$$

where

$$\left.\begin{aligned} &Ra = \frac{(1-C^*)(T_1-T^*)\beta g a^3}{\nu\alpha},\ M^2 = \frac{\sigma B_0^2 a^2}{\mu},\ \mathrm{Re} = \frac{aU_m}{\nu},\ \nu = \frac{\mu}{\rho},\ \mathrm{Pr} = \frac{\nu}{\alpha},\ \Lambda = \frac{K_r^2 a}{U_m}, \\ &Br = \frac{\mu U_m^2}{k(T_1-T^*)},\ Nb = \frac{\tau D_B(C_1-C^*)}{\alpha},\ Nr = \frac{(\rho_p-\rho_f)(C_1-C^*)}{\rho_f \beta(T_1-T^*)(1-C^*)},\ Rd = \frac{16\sigma^* T_1^3}{3k^* k}, \\ &S_c = \frac{\nu}{D_B},\ \delta = \frac{T_1-T^*}{T^*},\ E = \frac{E_a}{\kappa T^*},\ Nt = \frac{\tau D_T(T_1-T^*)}{T^*\alpha},\ \gamma = \frac{U_m a^2}{\alpha(T_1-T^*)}\frac{\partial \bar{T}}{\partial \bar{x}} = \text{constant}, \\ &Bi = \frac{h_f a}{k},\ Nj = \frac{h_s a}{D_B}. \end{aligned}\right\} \tag{20}$$

The skin-friction coefficient C_f with shear stress, Nusselt number Nu with heat transfer rate, and Sherwood number Sh with mass transfer rate are defined:

$$C_f = \frac{2\tau_w}{\rho U_m^2},\quad Nu = \frac{aq_w}{k(T_1 - T^*)},\quad Sh = \frac{aq_m}{D_B(C_1 - C^*)}, \tag{21}$$

where τ_w (sharing stress), q_w (heat transfer rate) and q_m (mass transfer rate) at the walls are describes as:

$$\begin{aligned}&\text{At upper wall}: \ \tau_w = -\mu\left(\frac{\partial \bar{u}}{\partial \bar{y}}\right)_{\bar{y}=a},\\ &q_w = -k\left(\frac{\partial \boldsymbol{T}}{\partial \bar{y}}\right)_{\bar{y}=a} \text{ and } q_m = -D_B\left(\frac{\partial \boldsymbol{C}}{\partial \bar{y}}\right)_{\bar{y}=a}\\ &\text{At lower wall}: \ \tau_w = -\mu\left(\frac{\partial \bar{u}}{\partial \bar{y}}\right)_{\bar{y}=-a},\\ &q_w = -k\left(\frac{\partial \boldsymbol{T}}{\partial \bar{y}}\right)_{\bar{y}=-a} \text{ and } q_m = -D_B\left(\frac{\partial \boldsymbol{C}}{\partial \bar{y}}\right)_{\bar{y}=-a}\end{aligned} \tag{22}$$

The non-dimensional C_f, Nu and Sh at the upper and upper walls are:

$$C_f = (2/\mathrm{Re})u'(y)|_{\substack{\bar{y}=1\\ \bar{y}=-1}} \quad Nu = -\theta'(y)|_{\substack{\bar{y}=1\\ \bar{y}=-1}} \quad \text{and} \quad Sh = -\phi'(y)|_{\substack{\bar{y}=1\\ \bar{y}=-1}} \tag{23}$$

Solution of problem

For the series solution: Initial guesses $u_0(y)$, $\theta_0(y)$, $\phi_0(y)$, linear operators $£_1(u)$, $£_2(\theta)$, $£_3(\phi)$ and auxiliary parameters $\hbar_u$, $\hbar_\theta$, $\hbar_\phi$ of velocity, temperature, concentration are defined respectively with embedding parameter $\xi \in [0, 1]$.

$$u_0(y) = \frac{U(1+y)}{2}, \quad \theta_0(y) = \frac{-1 + Bi(1-y)}{2Bi}, \quad \phi_0(y) = \frac{-1 + Nj(1-y)}{2Nj} \tag{24}$$

$$£_1 = u''(y), \quad £_2 = \theta''(y), \quad £_3 = \phi''(y). \tag{25}$$

Deformation problems at zeroth-order can be expressed as:

$$\left.\begin{aligned}(1-\xi)£_1[u(y,\xi) - u_0(y)] &= \xi\hbar_u N_u[u(y,\xi), \theta(y,\xi), \phi(y,\xi)],\\ (1-\xi)£_2[\theta(y,\xi) - \theta_0(y)] &= \xi\hbar_\theta N_\theta[u(y,\xi), \theta(y,\xi), \phi(y,\xi)],\\ (1-\xi)£_3[\phi(y,\xi) - \phi_0(y)] &= \xi\hbar_\phi N_\phi[u(y,\xi), \theta(y,\xi), \phi(y,\xi)].\end{aligned}\right\} \tag{26}$$

$$\left.\begin{array}{lll}\text{For} & \xi = 0 & \xi = 1\\ u(y,\xi): & u_0(y) & u(y)\\ \theta(y,\xi): & \theta_0(y) & \theta(y)\\ \phi(y,\xi): & \phi_0(y) & \phi(y)\end{array}\right\} \tag{27}$$

N_u, N_θ and N_ϕ are non-linear operators:

$$\left.\begin{aligned}&N_u[u(y,\xi), \theta(y,\xi), \phi(y,\xi)] = \tfrac{\partial^2 u(y,\xi)}{\partial y^2} - M^2 u(y,\xi)\\ &\quad + \tfrac{Ra}{\mathrm{RePr}}(\theta(y,\xi) - Nr\phi(y,\xi)) - P,\\ &N_\theta[u(y,\xi), \theta(y,\xi), \phi(y,\xi)] = (1 + R_d)\tfrac{\partial^2\theta(y,\xi)}{\partial y^2} + Nb\tfrac{\partial\theta(y,\xi)}{\partial y}\tfrac{\partial\phi(y,\xi)}{\partial y}\\ &\quad + Nt\left(\tfrac{\partial\theta(y,\xi)}{\partial y}\right)^2 + Br\left(\tfrac{\partial u(y,\xi)}{\partial y}\right)^2 + M^2Br(u(y,\xi))^2 - \gamma u(y,\xi),\\ &N_\theta[u(y,\xi), \theta(y,\xi), \phi(y,\xi)] = \tfrac{\partial^2\phi(y,\xi)}{\partial y^2}\\ &\quad - S_c\,\mathrm{Re}\Lambda(1 + \delta\theta(y,\xi))^{n_1}\left(-\tfrac{E}{(1+\delta\theta(y,\xi))}\right)\phi(y,\xi) + \tfrac{Nt}{Nb}\tfrac{\partial^2\theta(y,\xi)}{\partial y^2}.\end{aligned}\right\} \tag{28}$$

When embedding parameter ξ varies from 0 to 1, then $u\ (y, \xi)$, $\theta(y, \xi)$ and $\phi(y, \xi)$ change form initial guesses $u_0(y)$, $\theta_0\ (y)$ and $\phi_0\ (y)$ to desired $u\ (y)$, $\theta\ (y)$ and $\phi(y)$ solution.

Let us expand $u(y, \xi)$, $\theta(y, \xi)$ and $\phi(y, \xi)$ in Taylor's series as

$$\left.\begin{aligned}u(y,\xi) &= u_0(y) + \sum_{l=1}^{\infty} u_l(y)\,\xi^l,\\ \theta(y,\xi) &= \theta_0(y) + \sum_{l=1}^{\infty}\theta_l(y)\,\xi^l, \ .\\ \phi(y,\xi) &= \phi_0(y) + \sum_{l=1}^{\infty}\phi_l(y)\,\xi^l.\end{aligned}\right\} \tag{29}$$

In which

$$u_l(y) = \frac{1}{l!}\frac{\partial^l u(y,\xi)}{\partial\xi^l}\bigg|_{\xi=0}, \quad \theta_l(y) = \frac{1}{l!}\frac{\partial^l\theta(y,\xi)}{\partial\xi^l}\bigg|_{\xi=0}, \quad \phi_l(y) = \frac{1}{l!}\frac{\partial^l\phi(y,\xi)}{\partial\xi^l}\bigg|_{\xi=0}. \tag{30}$$

Now differentiate $l-$ times Eq. (26) to zeroth-order deformation w.r.t ξ and result divide by $l!$ then use $\xi = 0$ and obtained lth-order deformation expression for $u_l(y)$, $\theta_l(y)$ and $\phi_l(y)$ as follow:

$$\left.\begin{aligned}£_1[u_l(y) - \hat{\chi}_l u_{l-1}(y)] &= \hbar_u R_l^u(y),\\ £_2[\theta_l(y) - \hat{\chi}_l\theta_{l-1}(y)] &= \hbar_\theta R_l^\theta(y),\\ £_3[\phi_l(y) - \hat{\chi}_l\phi_{l-1}(y)] &= \hbar_\phi R_l^\phi(y),\end{aligned}\right\} \tag{31}$$

$$\left.\begin{aligned}&u_l(y,\xi) = U, \ \theta_l'(y,\xi) = -Bi(n - \theta_l(y,\xi)),\\ &\phi_l'(y,\xi) = -Nj(m - \phi_l(y,\xi)) \text{ at } \ y = 1\\ &u_l(y,\xi) = 0, \ \theta_l'(y,\xi) = -Bi(1 - \theta_l(y,\xi)),\\ &\phi_l'(y,\xi) = -Nj(1 - \phi_l(y,\xi)) \text{ at } y = -1\end{aligned}\right\} \tag{32}$$

$$\hat{\chi}_l = \begin{cases}0, & l \leqslant 1\\ 1, & l > 1\end{cases}. \tag{33}$$

$$\left.\begin{aligned}&R_l^u(y) = u_l'' - M^2u_l + \tfrac{Ra}{\mathrm{Re\,Pr}}(\theta_l - Nr\phi_l) - P,\\ &R_l^\theta(y) = (1 + Rd)\theta_l'' + Nb\sum_{k=0}^{l}\theta_k'\phi_{l-k}' + Nt\sum_{k=0}^{l}\theta_k'\theta_{l-k}'\\ &\qquad + Br\sum_{k=0}^{l}u_k'u_{l-k}' + M^2Br\sum_{k=0}^{l}u_lu_{l-k} - \gamma u_l,\\ &R_l^\phi(y) = \phi_l'' + \tfrac{Nt}{Nb}\theta_l'' - S_c\,\mathrm{Re}\Lambda(1 + \delta\theta_l)^{n_1}\exp\left(\tfrac{-E}{(1+\delta\theta_l)}\right)\phi_l.\end{aligned}\right\} \tag{34}$$

The lth-order approximation for solution can be stated as

$$\left.\begin{aligned}u(y) &= u_0(y) + \sum_{k=1}^{l}u_k(y),\\ \theta(y) &= \theta_0(y) + \sum_{k=0}^{l}\theta_k(y),\\ \phi(y) &= \phi_0(y) + \sum_{k=0}^{l}\phi_k(y).\end{aligned}\right\} \tag{35}$$

The analytical solution of velocity, temperature and nanoparticle concentration up to second order approximations are obtained for different values of pertinent parameters: $m = n = 0$, $Sc = 10$, $E = \delta = Rd = \Lambda = 1, M = 2.0$, $Ra = 2$, $\mathrm{Re} = 0.3$, $Nt = Nr = Nb = n_1 = Bi = Nj = 0.5$, $\gamma = 2$, and $\Pr = 7$ as given below:

$$u(y)=\frac{1}{2}+\frac{y}{2}+\hbar_u^2\left(\frac{254}{153}+\frac{2519y}{4590}-\frac{127y^2}{68}-\frac{1145y^3}{1836}+\frac{127y^4}{612}+\frac{229y^5}{3060}\right)+\hbar_u\left(\frac{127}{102}+\frac{229y}{306}-\frac{127y^2}{102}-\frac{229y^3}{306}+\hbar_\theta\left(-\frac{6685}{3672}-\frac{155y}{612}+\frac{275y^2}{153}+\frac{25y^3}{102}+\frac{25y^4}{1224}+\frac{5y^5}{612}+\frac{5y^6}{1836}\right)+\hbar_\phi\left(-\frac{13445}{19584}-\frac{12865y}{137088}+\frac{4405y^2}{6528}+\frac{1765y^3}{19584}+\frac{25y^4}{2176}+\frac{25y^5}{6528}+\frac{5y^6}{19584}+\frac{5y^7}{45696}\right)\right) \quad (36)$$

$$\theta(y)=-\frac{1}{2}-\frac{y}{2}+\hbar_\theta^2\left(\frac{1237}{480}+\frac{23y}{40}-\frac{y^2}{16}+\frac{13y^3}{48}+\frac{13y^4}{96}-\frac{y^5}{80}\right)+\hbar_\theta\left(\frac{22}{3}+3y+\frac{y^2}{2}+\frac{y^3}{3}+\frac{y^4}{6}+\hbar_u\left(\frac{127231}{36720}+\frac{34681y}{18360}+\frac{991y^2}{1224}+\frac{305y^3}{918}-\frac{533y^4}{7344}-\frac{991y^5}{6120}-\frac{229y^6}{4590}\right)+\hbar_\phi\left(\frac{3079}{2560}+\frac{769y}{1280}+\frac{353y^2}{2560}+\frac{3y^3}{128}+\frac{5y^4}{512}+\frac{y^5}{1280}-\frac{y^6}{2560}\right)\right) \quad (37)$$

$$\phi(y)=-\frac{1}{2}-\frac{y}{2}+\hbar_\phi^2\left(\frac{1381}{100}-\frac{6057y}{1000}-\frac{8649y^2}{5120}-\frac{2981y^3}{5120}+\frac{45y^4}{2048}+\frac{549y^5}{51200}-\frac{21y^6}{5120}+\frac{7y^7}{5120}+\frac{33y^8}{143360}-\frac{y^9}{20480}\right)+\hbar_\phi-\frac{881}{160}-\frac{353y}{160}-\frac{9y^2}{16}-\frac{5y^3}{16}-\frac{y^4}{32}+\frac{3y^5}{160}+\hbar_\theta\left(\frac{14299}{1920}+\frac{3421y}{840}+\frac{3y^2}{2}+\frac{11y^3}{48}-\frac{41y^4}{192}-\frac{3y^5}{40}-\frac{y^6}{240}-\frac{y^7}{336}-\frac{y^8}{896}\right). \quad (38)$$

Convergence analysis

HAM is a powerful method to solve the linear and highly non-linear problems. Here the Eq. (29) involve the auxiliary parameters $\hbar_u$, $\hbar_\theta$ and $\hbar_\phi$ is series solution. To choose the appropriate value of $\hbar_u$, $\hbar_\theta$ and $\hbar_\phi$, Fig. 2 depict ħ-curves at 25th order of approximations. It is observed that reliable values of the resulting solutions are lies in the range $-0.75 \leqslant \hbar_u \leqslant 0.2$, $-0.8 \leqslant \hbar_\theta \leqslant -0.1$ and $-0.55 \leqslant \hbar_\phi \leqslant 0.15$. According to Liao [30], the valid range of ħ lies in the flat portion of these curves. Moreover the series solutions are convergent in the entire zone of y, when $\hbar_u = \hbar_\theta = \hbar_\phi = -0.4$. Table 1 shows that the convergent series solution of velocity, temperature and concentration at different order approximation.

Results and discussion

In this portion the transmuted non-linear differential equations which are ODEs from (15) to (17) associated with the convective boundary conditions (18) and (19) were analytically solved by using Homotopy analysis method. The acts of different evolving parameters including Brownian motion parameter, radiation parameter, buoyancy ratio parameter, dimensionless activation energy, thermophoresis parameter, temperature difference parameter, fitted rate constant, Schmidt number, Brinkman number, non-dimensional reaction rate, Biot number and convection diffusion parameter on flow field, temperature distribution and concentration profile are discussed from Figs. 3–10.. The following discussion and results are obtained by using appropriate values of emerging parameters: $m = n = 0$, $U = 1$, $n_1 = 0.5$, $E = 1$, $\delta = 1$, $Sc = 10$, $M = 2.0$, $Ra = 2$, $\Lambda = 1$, $Rd = 1$, $\gamma = 2$, $Nb = 0.5$, $Nt = 0.5$, $\Pr = 7$, $\mathrm{Re} = 0.3$, $Br = 1$, $Nr = 0.5$, $Bi = 0.5$ and $Nj = 0.5$. Fig. 3a–c illustrate the collective influence of magnetic parameter M on velocity, temperature and concentration fields. As $M = 0$ leads hydrodynamic flow and $M \neq 0$ corresponds to hydromagnetic flow phenomena. It observed in Fig. 3a that velocity suppresses with increasing values of M due to increasing Lorentz forces which opposes the flow of nanofluid. It is also noted that temperature distribution is higher for hydromagnetic flow as compared to hydrodynamic flow case. Lorentz force is stronger for large magnetic field parameter. This stronger Lorentz force caused an enhancement in the temperature distribution as shown in Fig. 3b. Plot of concentration profile for different values of magnetic field parameter presented in Fig. 3c. The increasing result occur for concentration profile by M. The fluid motion is also affected by higher values of bouncy ratio parameter Nr, shown in Fig. 4. As enhancement in opposite bouncy caused by ambient nanoparticle volume fraction results in a decrease in velocity profile. Fig. 5 is drawn to depict the influence of radiation parameter Rd on temperature distribution. Increasing effect noted on the temperature distribution of nanofluid due to increase in radiation parameter. Physically, this enhancement occur when the radiative heat flux of the nanofluid increase in the channel.

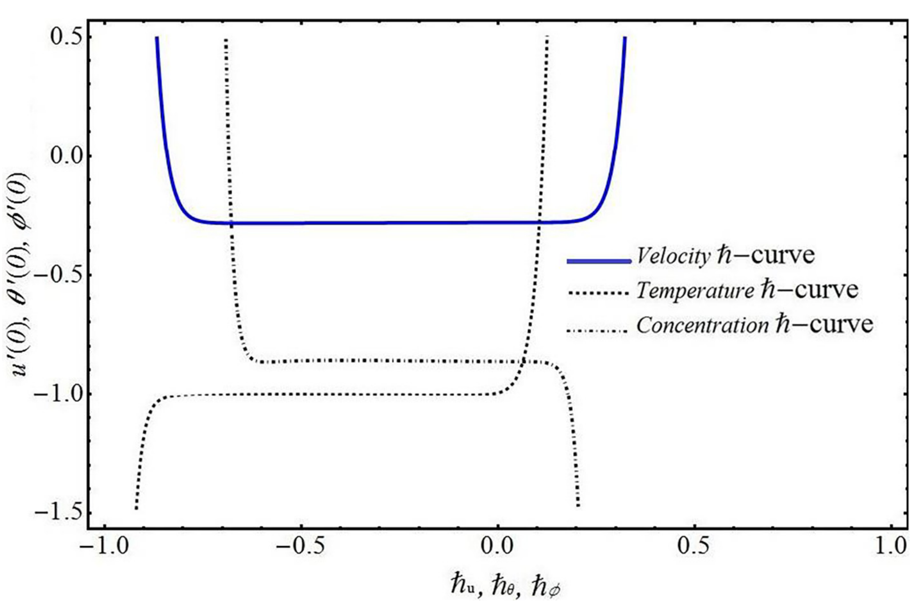

Fig. 2. ħ-curves for distributions up to 25{th}-order approximations.

Table 1
HAM solutions convergence when $m = n = 0$, $Sc = 10$, $E = \delta = Rd = \Lambda = 1$, $M = 2.0$, $Ra = 2$, $\mathrm{Re} = 0.3$, $Br = 1$, $Nt = Nr = Nb = n_1 = Bi = Nj = 0.5$, $\gamma = 2$ and $\mathrm{Pr} = 7$.

Order of approximation	Time	$-u'(y)$	$-\theta'(y)$	$-\phi'(y)$
1	3.45319	0.3688	1.0003	0.8873
5	25.84384	0.3681	0.9991	0.8865
11	64.2033	0.3673	0.9982	0.8857
18	157.7325	0.3664	0.9974	0.8849
22	214.2009	0.3657	0.9968	0.8842
25	380.2949	0.3657	0.9968	0.8842

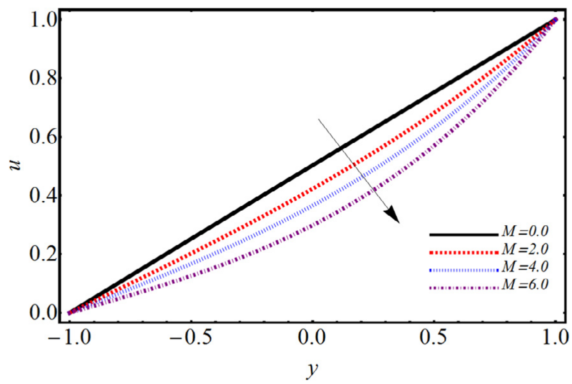

Fig. 3a. Effect of M on velocity profile.

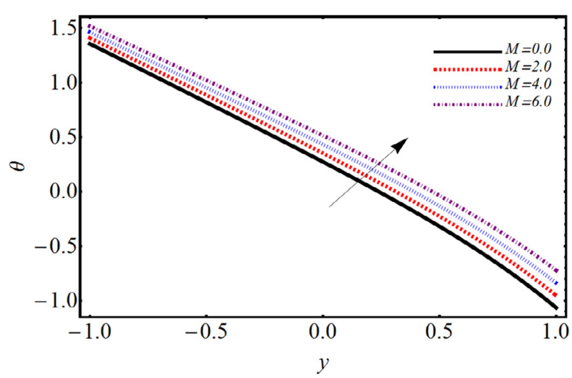

Fig. 3b. Effect of M on temperature profile.

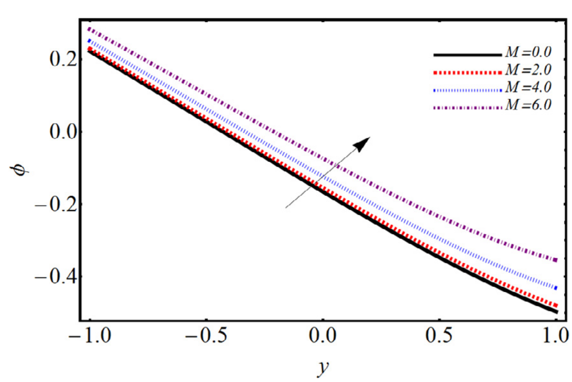

Fig. 3c. Effect of M on concentration profile.

Fig. 6a–c correspondingly show the velocity, temperature and concentration profiles for different values of chemical reaction parameter Λ. It is seen that the velocity profile increases with an increase in the chemical reaction parameter. It is also observed that when the chemical reaction parameter is negative (i.e. generative

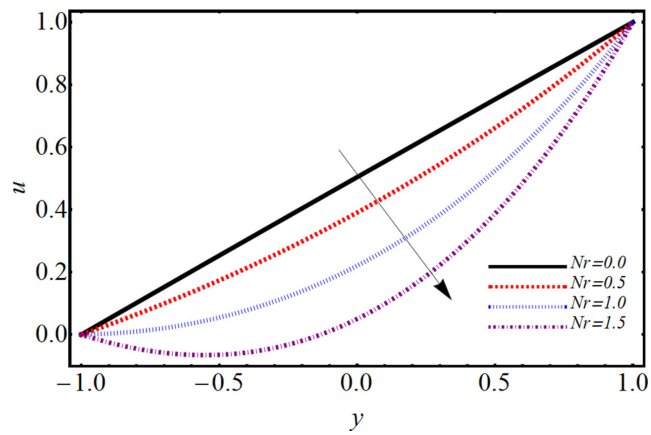

Fig. 4. Effect of Nr on velocity profile.

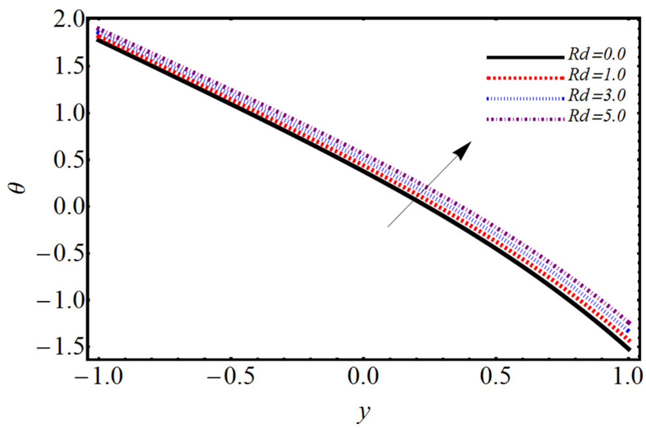

Fig. 5. Effect of Rd on temperature profile.

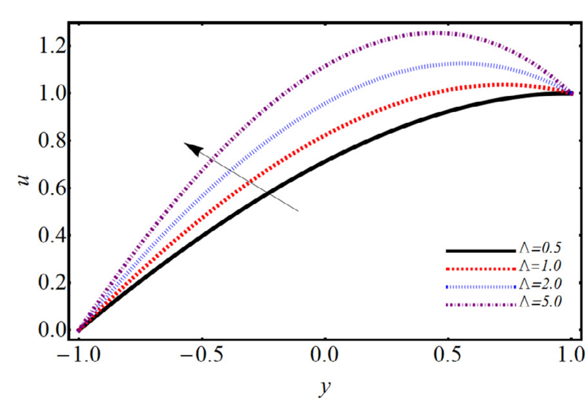

Fig. 6a. Effect of Λ on velocity profile.

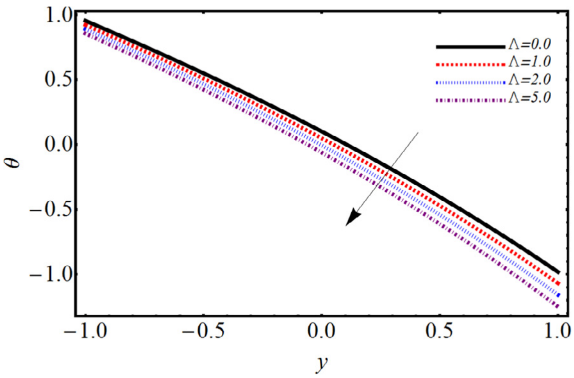

Fig. 6b. Effect of Λ on temperature profile.

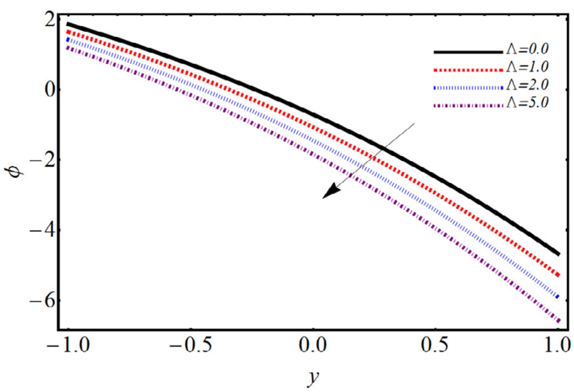

Fig. 6c. Effect of Λ on concentration profile.

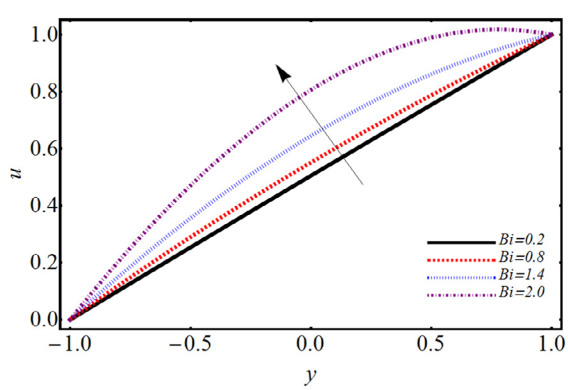

Fig. 7a. Effect of *Bi* on velocity profile.

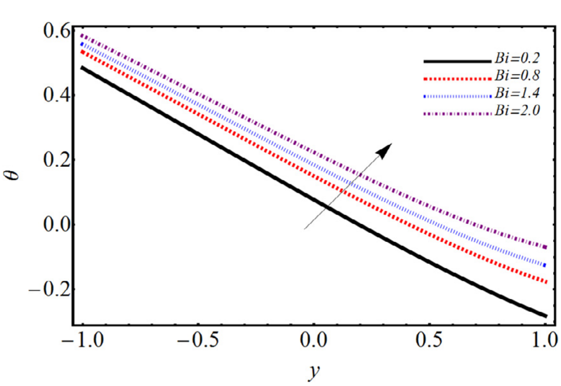

Fig. 7b. Effect of *Bi* on temperature profile.

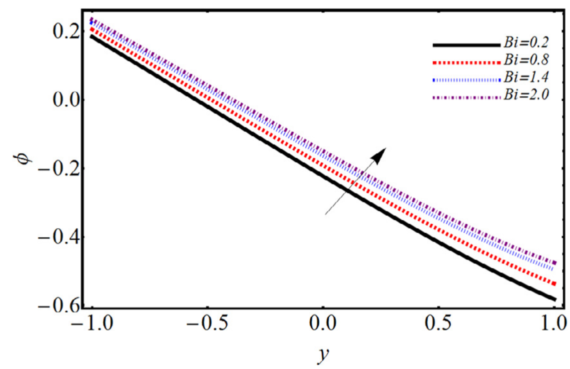

Fig. 7c. Effect of *Bi* on concentration profile.

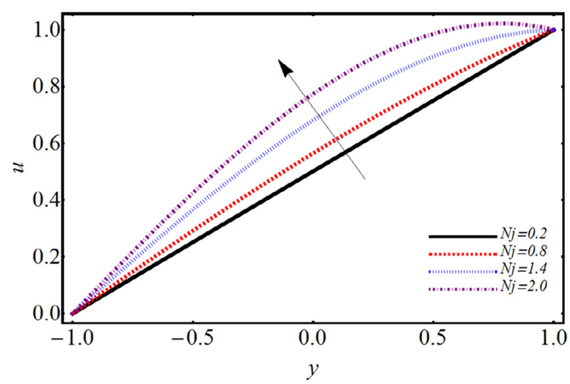

Fig. 8a. Effect of *Nj* on velocity profile.

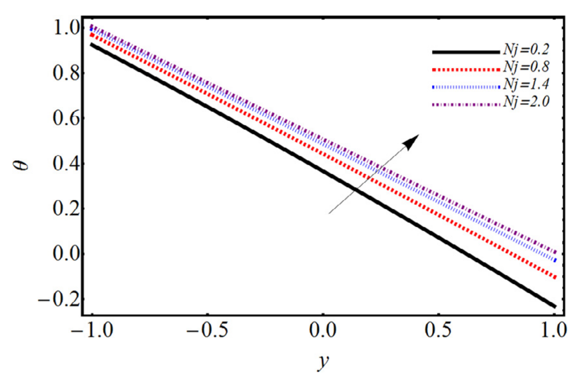

Fig. 8b. Effect of *Nj* on temperature profile.

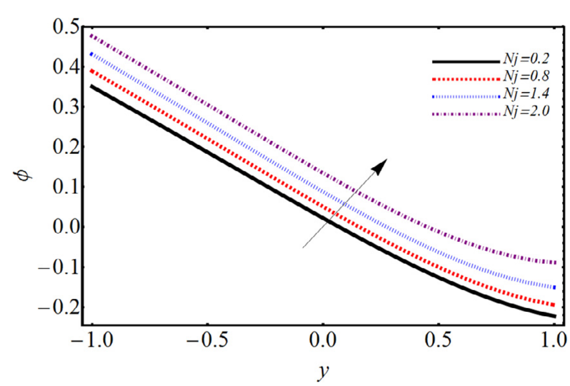

Fig. 8c. Effect of *Nj* on concentration profile.

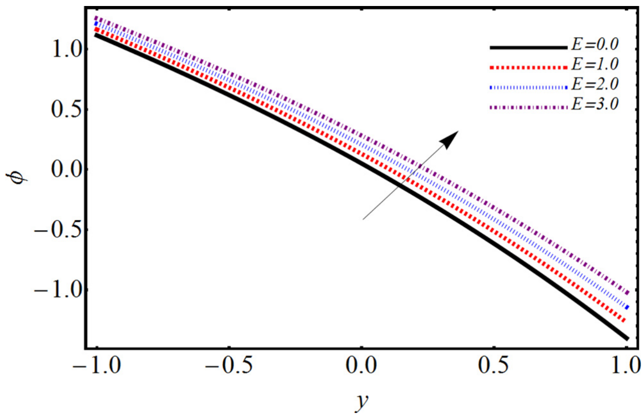

Fig. 9. Effect of E on concentration profile.

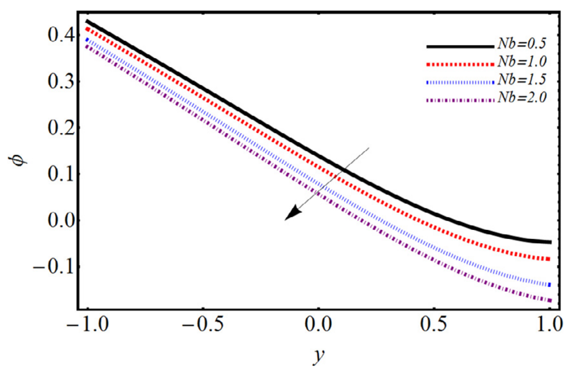

Fig. 10a. Effect of Nb on concentration profile.

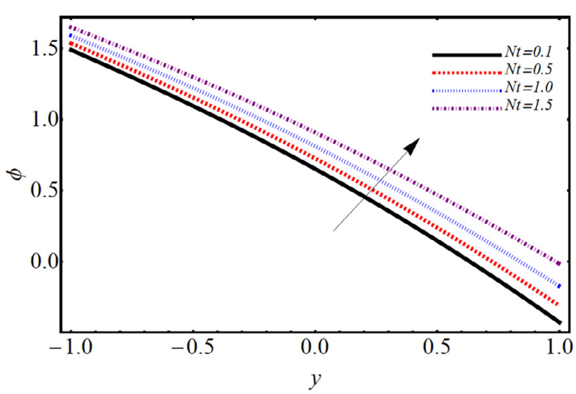

Fig. 10b. Effect of Nt on concentration profile.

reaction or $\Lambda < 0$) there is an increase in the fluid flow velocity. Physically, the amount of velocity reduces due to the chemical reaction but near the surface it gain the maximum amplitude as compare to the surface boundary For positive chemical reaction parameter (i.e. destructive reaction or $\Lambda > 0$), there is reduction in the fluid flow velocity. Moreover it can also be seen that the nanofluid temperature and volume concentration of nanoparticle are decelerated on increase of Λ. This behavior represent the weak effect of buoyancy force due to concentration gradient, which cause the reduction effect on concentration profile. The concentration fields are in good agreement with the outcomes found in case of Rout et al. [38]. Fig. 7a shows the velocity profile with or without Biot number. It is interesting to note that without Biot number (i.e. $Bi = 0$) the peak velocity is low. As the convection Biot number increases, the plate thermal resistance reduces. Consequently, the peak velocity and the velocities in the neighbourhood of the peak increase significantly. The effect of Biot number Bi (convection conduction parameter) on temperature can be observed in Fig. 7b. Since Bi is associated with heat transfer at the surface. The increase in Bi causes improvement in thermal boundary layer which yields increase in temperature. Fig. 7c depict the effects of Biot number Bi on concentration field. Concentration field and its associated boundary layer thickness are enhanced for the larger thermal Biot number Bi. The velocity profile for with and without convection-diffusion parameter is displayed in Fig. 8a. From the plot it can be noticed that when the convection–diffusion parameter is zero then the flow is smooth in the entire geometry, but when the values of convection-diffusion parameter increases then the velocity of nanofluid enhanced. The plots of temperature profile for different values convection-diffusion parameter Nj is exposed in Fig. 8b. Result shows in said figure gives the increasing effects in temperature with the increase of convection-diffusion parameter Nj. The influence of convection-diffusion parameter Nj on concentration distribution is presented in Fig. 8c, a strong increase in the concentration profile is achieved with increasing Nj values. Fig. 9 elucidates the increasing behavior in concentration profile due to increasing values of non-dimensional activation energy E which gives the large concentration of boundary layer thickness. Physically, higher activation energy and lower temperature leads to lesser reaction rate, which slows down the chemical reaction. In Figs. 10a–b expose the results on concentration profile in response to a variation in Brownian motion Nb and thermophoresis parameter Nt respectively. As the values of Brownian motion parameter increase, the concentration boundary layer thickness decrease, but the performance of thermophoresis parameter on nanoparticle concentration gives reverse pattern to that of Brownian motion parameter. In Tables 2–4 represents the numerical results of magnetic field parameter, buoyancy ratio parameter, Rayleigh number,

Table 2
Skin friction coefficient for several of M, Nr, Ra and Pr with $\mathrm{Re} = 0.3$, $Sc = 10$, $Rd = \Lambda = E = \delta = Br = 1$, $n_1 = Nt = Nb = Bi = Nj = 0.5$ for both walls.

M	Nr	Ra	Pr	$-u'(-1)$	$-u'(1)$
0.0	0.5	2	7	−0.004573	0.004745
2.0				−0.004044	0.004606
4.0				−0.003453	0.004187
6.0				−0.002801	0.003489
	0.5			−0.004044	0.004606
	1.0			−0.004251	0.005911
	1.5			−0.004457	0.007216
	2.0			−0.004664	0.008522
		1		−0.005388	0.006848
		2		−0.004044	0.004606
		3		−0.002700	0.002364
		4		−0.001356	0.000122
			7	−0.004044	0.004606
			8	−0.004380	0.005166
			9	−0.004642	0.005602
			10	−0.004851	0.005951

Table 3
Nusselt number for several of M, Nt, Rd, Nb and Br with $\mathrm{Re} = 0.3, Sc = 10$, $\mathrm{Pr} = 7$, $Ra = 2$, $\Lambda = E = \delta = 1$, $n_1 = Nr = Bi = Nj = 0.5$ for both walls.

M	Nt	Rd	Nb	Br	$-\theta'(-1)$	$-\theta'(1)$
0.0	0.5	1	0.5	1	0.492929	0.504004
2.0					0.493246	0.504333
4.0					0.493493	0.504745
6.0					0.493810	0.505321
	0.5				0.493246	0.504333
	1.0				0.494116	0.506943
	1.5				0.494990	0.509565
	2.0				0.495869	0.512199
		1			0.493246	0.504333
		2			0.493262	0.504369
		3			0.493278	0.504406
		4			0.493293	0.504442
			0.5		0.493246	0.504333
			1.0		0.493848	0.506208
			1.5		0.494451	0.508085
			2.0		0.495055	0.509964
				0	0.492212	0.501538
				1	0.493246	0.504333
				5	0.494280	0.507129
				7	0.495314	0.509924

Table 4
Sherwood number for several of $\Lambda, E, n_1, \delta, Sc$ and Rd with $\mathrm{Re} = 0.3$, $Sc = 10$, $\mathrm{Pr} = 7$, $Ra = 2$, $\Lambda = E = \delta = 1$, $n_1 = Nr = Bi = Nj = 0.5$ for both walls.

Λ	E	n_1	δ	Sc	Rd	$-\phi'(-1)$	$-\phi'(1)$
0.0	2.0	0.5	1.0	10.0	1.0	−0.744148	2.330771
1.0						−0.870893	2.552822
2.0						−1.007160	2.795660
5.0						−1.153320	3.060250
	0.0					−0.124560	1.082631
	1.0					−0.241022	1.606220
	2.0					−0.870893	2.552820
	3.0					−1.842190	4.057940
		−1.0				−3.411570	6.359712
		0.0				−1.512590	3.509851
		0.5				−0.870893	2.552823
		1.0				−0.397690	1.851932
	1.0		0.0		0.5	0.052703	0.356023
	1.0		1.0			0.409739	0.715164
	1.0		2.0			2.652001	2.867631
	1.0		3.0			9.993070	9.019430
	1.0			1.0		5.312660	2.974801
	1.0			3.0		6.700660	4.696381
	1.0			5.0		8.257800	6.704832
	1.0			10.0		9.993070	9.019430

radiation parameter, Prandtl number, Brownian motion parameter, Brinkman number, dimensionless reaction rate, non-dimensional activation energy, fitted rate constant, temperature difference parameter, thermophoresis parameter, Schmidt number, Biot number and convection diffusion parameter on skin friction coefficient, Nusselt number and Sherwood number respectively. The increasing behavior of Skin friction and Nusselt number are detected for magnetic field parameter, while the opposite trend observed on Sherwood number for activation energy.

Conclusions

The Current communication addresses the Couette-Poiseuille MHD radiative heat and mass transport with convective boundary conditions in horizontal channel using Buongiorno's model. Additionally, the impact of activation energy and chemical reaction are also taken into concentration field. The energy distribution along with the joule heating, viscous dissipation and radiation are also considered. The velocity of the nanofluid is generated due to constant pressure gradient in axial direction. The flow problem is first modeled and then transform into dimensionless form via appropriate similarity transformation. Homotopy Analysis Method (HAM) is utilized to tackle the resulting dimensionless flow problem. The acts of different evolving parameters including Brownian motion parameter, radiation parameter, buoyancy ratio parameter, dimensionless activation energy, thermophoresis parameter, temperature difference parameter, fitted rate constant, Schmidt number, Brinkman number, non-dimensional reaction rate, Biot number and convection diffusion parameter on fluid velocity, temperature distribution, skin friction coefficient, Nusselt number and Sherwood number are expressed for nanofluid through figures and tabular forms. The key outcomes of the problem can be comprehended as follows:

- Heat and mass distribution gives the proportionally effects with the magnetic field parameter as compare to flow field.
- It is perceived that the velocity of nanofluid decelerate by increasing the values of modified magnetic parameter, whereas the temperature and concentration profile is increased by increasing the said parameters.
- Inverse behavior captured in heat and mass distribution with influence of chemical reaction.

- Activation energy gives the same agreement with the concentration field.
- Shear effects on both walls gives the opposite effects due to increase in buoyancy ratio and magnetic parameter.
- The increasing effects of Heat transfer on both walls has detected with respect to thermophoresis and magnetic field parameter.
- Activation energy and chemical reaction give the opposite trend on channel walls for Sherwood number.

Appendix A. Supplementary data

Supplementary data associated with this article can be found, in the online version, at https://doi.org/10.1016/j.rinp.2017.12.024.

References

[1] Buongiorno J. Convective transport in nanofluids. J Heat Transfer 2006;128:240–50.
[2] Choi SU. Enhancing thermal conductivity of fluids with nanoparticles. ASME-Publications-Fed 1995;231:99–106.
[3] Sheikholeslami M, Ganji DD. Numerical approach for magnetic nanofluid flow in a porous cavity using CuO nanoparticles. Mater Desg 2017;120:382–93.
[4] Rashidi MM, Hakeem AA, Ganesh NV, Ganga B, Sheikholeslami M, Momoniat E. Analytical and numerical studies on heat transfer of a nanofluid over a stretching/shrinking sheet with second-order slip flow model. Int J Mech Mater Eng 2016;11. https://doi.org/10.1080/14484846.2017.1358844.
[5] Shehzad N, Zeeshan A, Ellahi R, Vafai K. Convective heat transfer of nanofluid in a wavy channel: Buongiorno's mathematical model. J Mol Liq 2016;222:446–55.
[6] Xu H, Fan T, Pop I. Analysis of mixed convection flow of a nanofluid in a vertical channel with the Buongiorno mathematical model. Int Commun Heat Mass Transfer 2013;44:15–22.
[7] Zeeshan A, Maskeen MM, Mehmood OU. Hydromagnetic nanofluid flow past a stretching cylinder embedded in non-Darcian Forchheimer porous media. Neural Comput Appl 2017. https://doi.org/10.1007/s00521-017-2934-7.
[8] Zeeshan A, Shehzad N, Ellahi R, Alamri SZ. Convective Poiseuille flow of Al2O3-EG nanofluid in a porous wavy channel with thermal radiation. Neural Comput Appl 2017. https://doi.org/10.1007/s00521-017-2924-9.
[9] Ellahi R, Hassan M, Zeeshan A. Shape effects of spherical and non-spherical nanoparticles in mixed convection flow over a vertical stretching permeable sheet. Mech Adv Mater Struct 2017. https://doi.org/10.1080/15376494.2016.1232454.
[10] Sheikholeslami M, Bhatti MM. Forced convection of nanofluid in presence of constant magnetic field considering shape effects of nanoparticles. Int J Heat Mass Transfer 2017;111:1039–49.
[11] Muhammad N, Nadeem S, Mustafa T. Squeezed flow of a nanofluid with Cattaneo-Christov heat and mass fluxes. Results Phys 2017;7:862–9.
[12] Abbas T, Ayub M, Bhatti MM, Rashidi MM, Ali ME. Entropy generation on nanofluid flow through a horizontal Riga plate. Entropy 2016;18(6):223.
[13] Kumar R, Sood S, Shehzad SA, Sheikholeslami M. Numerical modeling of time-dependent bio-convective stagnation flow of a nanofluid in slip regime. Results Phys 2017;7:3325–32.
[14] Sheikholeslami M. Magnetic field influence on CuO–H2O nanofluid convective flow in a permeable cavity considering various shapes for nanoparticles. Int J Hydrogen Energy 2017;42(31):19611–21.
[15] Bhatti MM, Rashidi MM, Pop I. Entropy Generation with nonlinear heat and Mass transfer on MHD Boundary Layer over a Moving Surface using SLM. Nonlinear Eng Model App 2017;6(1):43–52.
[16] Rashidi MM, Ali M, Freidoonimehr N, Rostami B, Hossain MA. Mixed convective heat transfer for MHD viscoelastic fluid flow over a porous wedge with thermal radiation. Adv Mech Eng 2014;6:735939.
[17] Rashidi MM, Abelman S, Mehr NF. Entropy generation in steady MHD flow due to a rotating porous disk in a nanofluid. Int J Heat Mass Transfer 2013;62:515–25.
[18] Ramesh GK, Gireesha BJ. Influence of heat source/sink on a Maxwell fluid over a stretching surface with convective boundary condition in the presence of nanoparticles. Ain Shams Eng J 2014;5:991–8.
[19] Alsaedi A, Awais M, Hayat T. Effects of heat generation/absorption on stagnation point flow of nanofluid over a surface with convective boundary conditions. Commun Nonlinear Sci Numer Simul 2012;17:4210–23.
[20] Zeeshan A, Majeed A, Fetecau C, Muhammad S. Effects on heat transfer of multiphase magnetic fluid due to circular magnetic field over a stretching surface with heat source/sink and thermal radiation. Results Phys 2017;7:3353–60.
[21] Hamad MA, Uddin MJ, Ismail AM. Radiation effects on heat and mass transfer in MHD stagnation-point flow over a permeable flat plate with thermal convective surface boundary condition, temperature dependent viscosity and thermal conductivity. Nucl Eng Des 2012;242:194–200.
[22] Lopez A, Ibanez G, Pantoja J, Moreira J, Lastres O. Entropy generation analysis of MHD nanofluid flow in a porous vertical microchannel with nonlinear thermal radiation, slip flow and convective-radiative boundary conditions. Int J Heat Mass Transfer 2017;107:982–94.
[23] Bestman AR. Natural convection boundary layer with suction and mass transfer in a porous medium. Int J Energy Res 1990;14:389–96.
[24] Maleque K. Effects of binary chemical reaction and activation energy on MHD boundary layer heat and mass transfer flow with viscous dissipation and heat generation/absorption. ISRN Thermodyn 2013. https://doi.org/10.1155/2013/284637.
[25] Mustafaa M, Hayat T, Obaidat S. Boundary layer flow of a nanofluid over an exponentially stretching sheet with convective boundary conditions. Int J Numer Methods Heat Fluid Flow 2013;23:945–59.
[26] Mohyud-Din ST, Khan U, Ahmed N, Bin-Mohsin B. Heat and mass transfer analysis for MHD flow of nanofluid in convergent/divergent channels with stretchable walls using Buongiorno's model. Neural Comput Appl 2017;28:4079–92.
[27] Rassoulinejad-Mousavi SM, Seyf HR, Abbasbandy S. Heat transfer through a porous saturated channel with permeable walls using two-equation energy model. J Porous Media 2013;3:241–54.
[28] Awad FG, Motsa S, Khumalo M. Heat and mass transfer in unsteady rotating fluid flow with binary chemical reaction and activation energy. PLoS One 2014;9. https://doi.org/10.1371/journal.pone.0107622.
[29] Shafique Z, Mustafa M, Mushtaq A. Boundary layer flow of Maxwell fluid in rotating frame with binary chemical reaction and activation energy. Results Phys 2016;6:627–33.
[30] Liao SJ. The proposed homotopy analysis technique for the solution of nonlinear problems [Ph.D. thesis]. Shanghai Jiao Tong University; 1992.
[31] Zhao Y, Liao S. HAM-based mathematica package BVPh 2.0 for nonlinear boundary value problems. Adv Homotopy Anal Method 2013;361.
[32] Rashidi MM, Domairry G, Dinarvand S. Approximate solutions for the Burger and regularized long wave equations by means of the homotopy analysis method. Commun Nonlinear Sci 2009;14(3):708–17.
[33] Mustafa M, Khan JA, Hayat T, Alsaedi A. Buoyancy effects on the MHD nanofluid flow past a vertical surface with chemical reaction and activation energy. Int J Heat Mass Transfer 2017;108:1340–6.
[34] Revnic C, Grosan T, Pop I, Ingham DB. Magnetic field effect on the unsteady free convection flow in a square cavity filled with a porous medium with a constant heat generation. Int J Heat Mass Transfer 2011;54:1734–42.
[35] Tencer M, Moss JS, Zapach T. Arrhenius average temperature: the effective temperature for non-fatigue wear out and long term reliability in variable thermal conditions and climates. IEEE Trans Compon Packag Technol 2004;27:602–7.
[36] Kuznetsov AV, Nield DA. Natural convective boundary-layer flow of a nanofluid past a vertical plate. Int J Thermal Sci 2010;49:243–7.
[37] Zhang C, Zheng L, Zhang X, Chen G. MHD flow and radiation heat transfer of nanofluids in porous media with variable surface heat flux and chemical reaction. Appl Math Model 2015;39:165–81.
[38] Rout BR, Parida SK, Pattanayak HB. Effect of radiation and chemical reaction on natural convective MHD flow through a porous medium with double diffusion. J Eng Thermophys 2014;23:53–65.